Bulk-heterojunction solar cells with enriched polymer contents

Yin, Hang; Chiu, Ka Lok; Ho, Carr Hoi Yi; Lee, Harrison Ka Hin; Li, Ho Wa; Cheng, Yuanhang; Tsang, Sai Wing; So, Shu Kong

Published in:
Organic Electronics

DOI:
10.1016/j.orgel.2016.10.030

Published: 01/01/2017

Document Version:
Peer reviewed version

Bulk-heterojunction Solar Cells with Enriched Polymer Contents

*Hang Yin, Ka Lok Chiu, Carr Hoi Yi Ho, Harrison Ka Hin Lee, Ho Wa Li, Yuanhang Cheng, Sai Wing Tsang, and Shu Kong So**

H. Yin, K. L. Chiu, C. H. Y. Ho, Dr. H. K. H. Lee, Prof. S. K. So

Department of Physics and Institute of Advanced Materials

Hong Kong Baptist University

Kowloon Tong, Hong Kong SAR, P.R. China

E-mail: skso@hkbu.edu.hk

H. W. Li, Y. Cheng, Dr. S. W. Tsang

Department of Physics and Materials Science

City University of Hong Kong

Kowloon Tong, Hong Kong SAR, P. R. China

Keywords: donor:acceptor ratio, PCE, charge transport, admittance spectroscopy

Abstract: In a high performance PTB7:$PC_{71}BM$ bulk-heterojunction (BHJ) solar cell, the commonly optimized polymer:fullerene (D:A) weight ratio is about 1:1.5, when $PC_{71}BM$ is used as the acceptor. This report explores alternative D:A weight ratios. We describe how to enrich the polymer contents of these BHJ solar cells to achieve high power conversion efficiencies (PCEs). The concentration of 1,8-diiodooctane (DIO), a solvent additive for the

BHJ precursor solutions, is increased in order to re-optimize the BHJ cells. The PCEs of the re-optimized cells are improved for the PTB7 cells. Detailed charge transport measurements were carried out to examine the polymer-rich BHJs. We observed enhanced hole mobilities for the PTB7 BHJs. Additionally, the electron mobilities are preserved due to the dispersion of fullerene domains by increased DIO concentrations. Two other well-known polymer donors PCDTBT and PDTSTPD have been also investigated, and the improvements of hole mobilities and PCEs can be obtained for both polymer-rich BHJ solar cells.

1. Introduction

Organic photovoltaic (OPV) cells have attracted tremendous attentions.[1-5] They are light, flexible, and have huge potential in large area fabrication by roll-to-roll processing.[6-8] In a polymer-based OPV cell, the polymer acts as the light absorber, electron donor, and hole transporter, whereas fullerene molecules typically have less optical absorption and mainly serve as electron acceptors and transporters.[9] If the polymer and fullerene are blended together intimately, the resulting bulk heterojunction (BHJ) is a very effective active layer for optical absorption and charge carrier transport.[10-12] Among many tested BHJs, the PTB7:$PC_{71}BM$ BHJ blend with 1,8-diiodooctane (DIO) as the additive in casting solution is one of the well-studied and efficient OPV systems.[13,14,15] A certified power conversion efficiency (PCE) of 9.2% has been reported.[16] Other BHJ devices such as PCDTBT:$PC_{71}BM$ and PDTSTPD:$PC_{71}BM$ have been reported with the PCEs of 6.1% and 7.3%.[10,17] Of the BHJs listed above, the optimal donor-acceptor (D:A) weight ratios are all larger than 1:1. However, the fullerene acceptors have weak absorbances in solar spectrum. Therefore, it should be highly desirable to enrich the polymer content in the BHJ in order to harvest more

photon energy. Furthermore, a higher polymer content should improve hole transport, lead to better balance of electron and hole mobilities, and improve the PCE.

Recently, novel polymers have been designed to accomplish BHJs with high polymer contents. Qian *et al.* designed a novel polythiophene derivative (PBT1).[18] With a D:A ratio of 1:0.66, an impressive PCE of 6.88% was achieved. More recently, Yuan *et al.* synthesized a polymer PTP8 with a high V_{oc} (~ 1.0V) and PCE of 6%.[19] The D:A weight ratio is 1:0.5. In both of these examples, the main strategy for reducing the content of fullerene is to reduce the free volume between the side chains of the high performance polymers. As proposed previously by McGehee et.al.[20], large spacings in between side chains may be conducive to fullerene intercalations and lead to a high level of fullerene loading. Thus, dense polymer side-chains should be able to suppress fullerene loading without compromising the power conversion efficiencies. This concept was realized from References 18 and 19, using bulky and rigid side chains.

In this report, we adopt a different strategy to realize OPV cells with enhanced polymer contents. We employ a well-known BHJ system PTB7:$PC_{71}BM$ and explore how to fabricate polymer-rich OPV devices with better performances. The chemical structures of the materials are shown in **Figure 1**. Our general strategy is as follows. *Due to increased polymer content, the reduced fullerene concentration in the BHJ is expected to suppress electron mobilities. To compensate this effect, we increase the DIO additive concentration in the processing solution. Although the fullerene concentration is reduced, a higher DIO concentration further disperses the fullerene domains, and helps to retain the electron mobility for electron extraction.* With this strategy, we re-optimized the BHJs which have enriched polymer

contents. For the BHJs using PTB7 as the donor polymer, their polymer-rich solar cells have improved PCEs relative to their reference cell. To look into the origins of the improved PCEs for the polymer-rich cells, we investigate the optical and transport properties of the BHJ films. The polymer-rich BHJ film exhibits an improved optical absorption and hole mobility. The polymer-rich strategy also works for other two BHJ systems based on PCDTBT:$PC_{71}BM$ and PDTSTPD:$PC_{71}BM$. The enhancements of PCE, hole mobility and UV-visible optical absorption can be also observed in both devices with higher polymer contents. Our results provide insight on the existing limitation of D:A ratio on the photovoltaic performance, and suggest alternatives to optimize the BHJ devices.

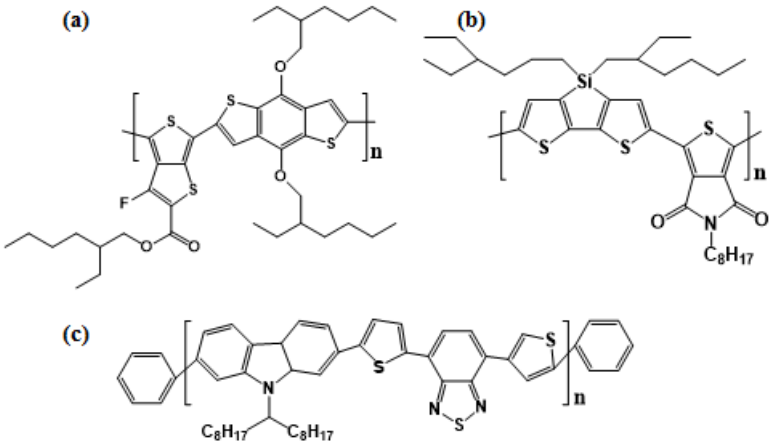

Figure 1. Chemical structures of (a)PTB7, (b)PCDTBT, (c)PDTSTPD

2. Result and Discussion

2.1. Impacts of Donor-acceptor Ratio on OPV Devices Performance

Figure 2(a) shows the current-voltage (J-V) characteristics of optimized PTB7:$PC_{71}BM$ bulk-heterojunction OPV devices with different donor-acceptor mass ratios under

100mWcm^{-2} AM1.5G illumination. The polymer-rich device was processed from a casting solution consisting of higher DIO additive concentrations for the balance of carrier mobilities. For the PTB7:$PC_{71}BM$ solar cells, 4 vol% DIO additive was doped into the casting solution of the polymer-rich (1:1 D:A mass ratio) devices, comparing with only 3 vol% DIO in the casting solution of the control devices (1:1.5 D:A mass ratio). The PCE of the polymer-rich cell can be found to be enhanced by a factor of 10%, from a control device with a PCE of 7.0% to 7.7%. The J_{sc} is the main contribution of the PCE enhancement, increasing from 15.1 mA/cm^2 of the control device to 16.8 mA/cm^2 of the polymer-rich device. However, the V_{oc} and FF have no significant changes in both D:A ratio devices with various DIO concentrations. **Table 1** lists the performances of the polymer-rich and control PTB7:$PC_{71}BM$ devices. Our result suggests that the polymer:fullerene OPV solar cell can be fabricated with reduced fullerene content. The J_{sc} of device can be improved by the reduction of $PC_{71}BM$ content with a higher DIO concentration in casting solution. The optimization procedures of PTB7:$PC_{71}BM$, and other two D:A systems in Section 2.3., involving PCDTBT:$PC_{71}BM$ and PDTSTPD:$PC_{71}BM$ OPV devices with various D:A ratios and DIO concentrations are shown in **Table S1**.

Figure 2(b) shows the external quantum efficiency (EQE) spectra of the PTB7:$PC_{71}BM$ devices with different D:A ratios. The optimized thickness of PTB7:$PC_{71}BM$ bulk-heterojunction active layer is around 90 nm, where the PCE performance is the best for the organic solar cells. The polymer-rich device shows an EQE enhancement in the wavelength region from 530 nm to 800 nm, in which PTB7 mainly contributes the light absorption. The EQE of the polymer-rich cell maintains above 70% from 490 nm until 695

nm, while that of the control cell decreases gradually to only 56% in 700 nm. **Figure 2(c)** shows the UV-visible absorption spectra of the PTB7 BHJs. The polymer-rich BHJ film has an distinct enhanced absorbance from 500-700 nm arising from the enhanced polymer content, when compared to the control sample (D:A ratio of 1:1.5).

In order to understand how the polymer fraction impacts on the carrier transport characteristics, hole-only devices were fabricated for the J-V measurements. The general device structure is ITO/PEDOT:PSS/BHJ/CuPc:spiro-TPD/Au. The PEDOT:PSS layer plays the role of the hole injection layer. The electron blocking layer (EBT) is a mixed layer of spiro-TPD and CuPc in a ratio of 30:1.[21,22] The JV data of PTB7:$PC_{71}BM$ hole-only devices at room temperature are shown in **Figure 2(d)**. The hole mobilities of the BHJs can be obtained by the space-charge-limited current (SCLC) equation: [23-25]

$$J_{SCL}d = \frac{9}{8}\varepsilon_0\varepsilon_r\mu_0\exp(0.89\beta\sqrt{F})F^2 \qquad (1)$$

where J_{SCL} is the space-charged-limited current density, d is the thickness of the BHJ film, ε_0 is the permittivity of a vacuum, ε_r is the relative permittivity of the polymer, μ_0 is the zero-field mobility, β is the field-dependent coefficient, and F is the average electrical field. It can be seen that the polymer-rich BHJ has an enhanced hole current with respect to the control devices, and therefore the hole mobility. It increases gradually from around 1.3×10^{-4} $cm^2V^{-1}s^{-1}$ to around 2.2×10^{-4} $cm^2V^{-1}s^{-1}$, when the D:A ratio increases from 1:1.5 to 1:1. Table 1, last column, is a summary of the SCLC fittings.

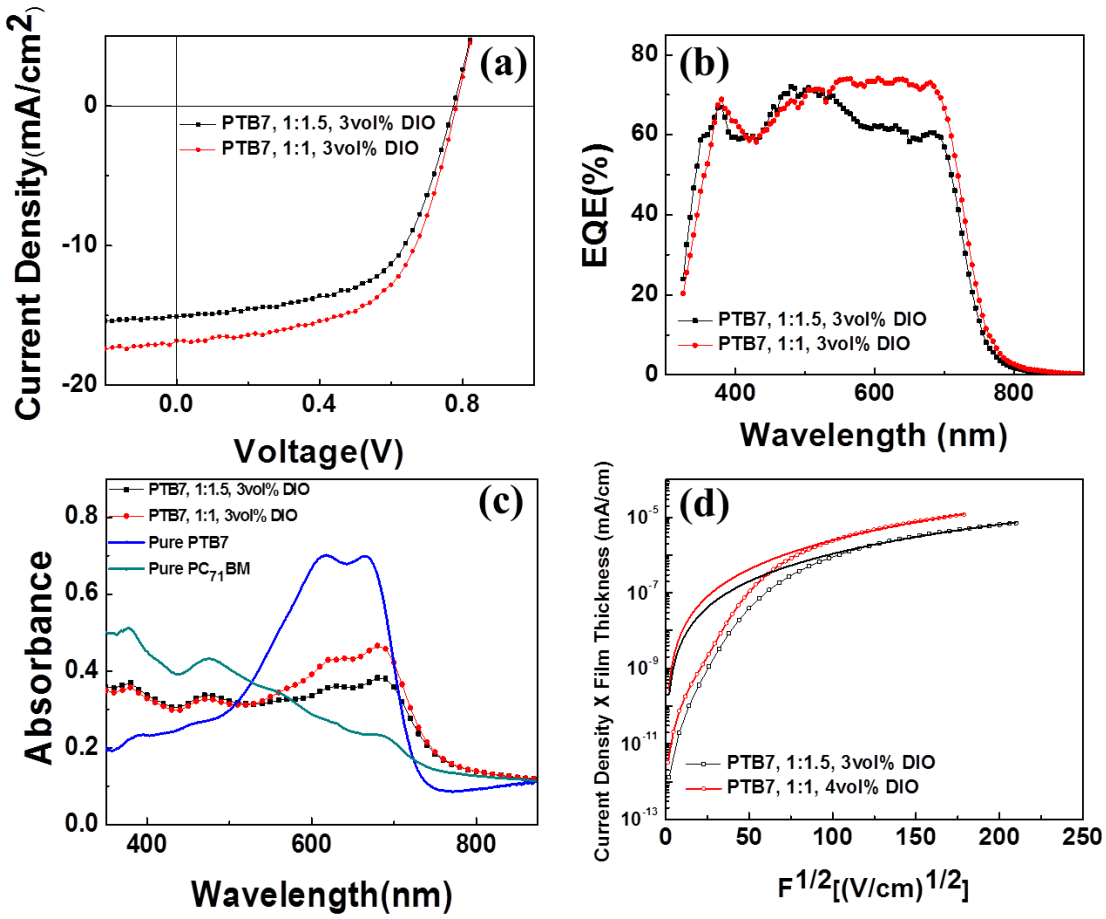

Figure 2. (a) JV data of typical PTB7:$PC_{71}BM$ bulk-heterojunction OPV devices under 100 mW/cm^2 of AM1.5G solar illumination. The data points in circles indicate BHJ cells with enhanced polymer contents; the data points in squares are the control devices. The D:A ratios are indicated in each plot; (b) EQE spectra for PTB7:$PC_{71}BM$ BHJ OPV devices; (c) UV-visible absorption spectra for PTB7:$PC_{71}BM$ BHJ films and materials absorption spectra with thicknesses similar to their BHJ cells; (d) Current vs applied field data for PTB7:$PC_{71}BM$ BHJ hole-only devices at room temperature. Circles are data for the polymer-rich samples while squares are data for the control devices. Solid lines are SCLC fittings using Equation 1.

BHJ	D:A weight ratio	DIO concentration (in vol%)	J_{sc} (mA/cm^2)	V_{oc} (V)	FF (%)	PCE (%)	μ_0(cm^{2}V^{-1}s^{-1})
PTB7: $PC_{71}BM$	1:1	4	16.8	0.78	59	7.7	2.2×10^{-4}
	1:1.5	3	15.1	0.77	60	7.0	1.3×10^{-4}

Table 1. Summary of performances of bulk-heterojunction OPV devices for different D:A ratios using PTB7 as the donor polymers. The last column indicates the hole mobilities obtained from SCLC fittings (Equation 1) to the JV data.

2.2. Electron and Hole Transports Measurements of Polymer-rich BHJ of PTB7:$PC_{71}BM$

To probe further the carrier transport properties, we use PTB7:$PC_{71}BM$ system as a model system and employ admittance spectroscopy (AS) to study the detailed charge transports of the BHJ films.[26-30] Particularly, in this report, AS was chosen for identifying the mechanism of how the D:A ratio and the DIO concentration affect carrier transports in the active layer. Both electron and hole transports were examined. The basic structure for hole-only devices is ITO/PEDOT:PSS/PTB7:$PC_{71}BM$/CuPc:spiro-TPD/Au, while the structure of electron-only device is ITO/Al/BHJ/LiF/Al. The operating principles of AS to extract carrier mobilities have been fully documented elsewhere.[27-29] (Appendix 1)

First, we examine how DIO concentrations in the processing solution influence both the electron and hole mobilities in a polymer-rich BHJ of PTB7:$PC_{71}BM$ (1:1) (**Figure 3**). The electron mobilities increase rapidly as the DIO concentration increases in the casting solution.

Without additives in the casting solution, the electron mobilities have values between 1.5 to 5.5×10^{-5} $cm^2V^{-1}s^{-1}$ as the electric field increases. The field dependent electron mobility can be described by the Poole-Frenkel (PF) model, i.e.,

$$\mu_e(F) = \mu_{0,e}\exp(\beta_e F^{1/2}) \quad (2)$$

where $\mu_{0,e}$ is the zero-field electron mobilities and β is the associated PF slope.[31] For the sample prepared with 10 vol% DIO, the electron mobility is in range of about 7.1 to 8.2×10^{-4} $cm^2V^{-1}s^{-1}$, which is almost 30 times larger than the case in which DIO is absent in the casting solution. The enhanced electron mobility with increasing DIO concentration is also supported by AFM investigations. As shown in the atomic force microscopy (AMF) images in **Figure S1** in the Supplementary Information, smaller fullerene aggregations occur when DIO is added to the BHJ of PTB7:$PC_{71}BM$. Reduced fullerene domain sizes are known to be favorable for electron transports because of reduced average hopping distances.[22] Our results indicate DIO concentration can be used to tune the electron mobility in a BHJ.

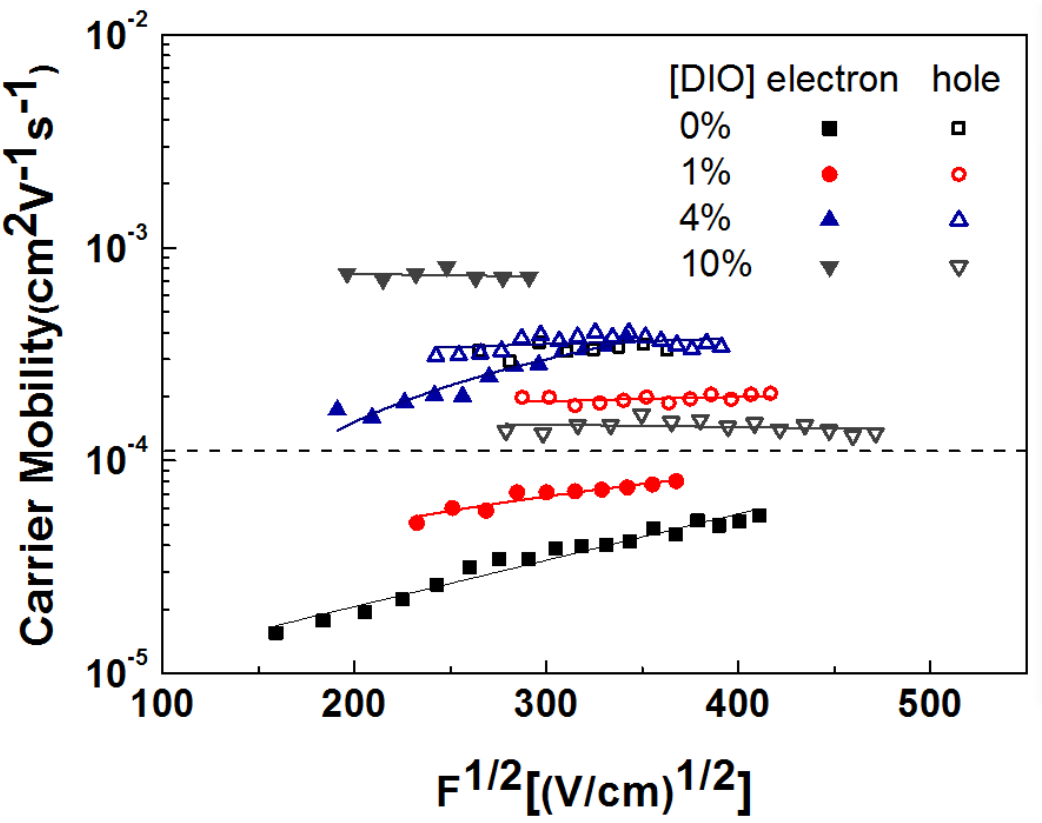

Figure 3. Effects of DIO concentrations in the casting solution on the electron and hole mobilities at room temperature for the BHJ films of PTB7:$PC_{71}BM$ with a D:A ratio of 1:1. The dashed line shows the hole mobility of a control device with a D:A ratio of 1:1.5. It can be observed that hole mobilities are generally field independent, and are consistently higher in the polymer-rich samples than the controls.

Figure 3 also show the hole mobility data for samples prepared with different DIO concentrations for the polymer-rich samples. In contrast to the electron data, hole mobilities are not so sensitive to the DIO concentration. The hole mobilities are nearly field independent, and they span a narrow range between $1\text{-}4\times10^{-4}$ $cm^2V^{-1}s^{-1}$. All polymer-rich hole-only devices with various DIO concentrations have larger hole mobilities than those of the control devices which have hole mobilities of about 1×10^{-4} $cm^2V^{-1}s^{-1}$. The dashed line in Figure 3

indicates the hole mobility of a typical control device with a D:A ratio of 1:1.5. We also note that for a DIO concentration of 4%, both electron and hole acquire nearly the same mobilities, with $\mu_e \approx \mu_h \approx 3 \times 10^{-4}$ $cm^2V^{-1}s^{-1}$.

The low-field mobilities at different temperatures can be further analyzed with the Gaussian disorder model (GDM). From the GDM, the low-field mobilities are related to temperature by

$$\mu_0 = \mu_\infty exp\left[-\left(\frac{2\sigma}{3kT}\right)^2\right] \quad (3)$$

where σ is the energetic disorder, μ_∞ represents the high temperature carrier mobility, k is the Boltzmann constant. μ_∞ can be obtained from the plot of μ_0 against $1/T^2$.[32] **Figure 4** shows such an analysis for both electrons and holes. The results show that the low-field mobilities are in good general agreements with Equation 3. The hole mobilities of the devices are insensitive to DIO concentrations. However, the hole mobility at a given temperature is higher than the control samples. The hole mobility of the 4 vol% DIO polymer-rich device is 3.8×10^{-5} $cm^2V^{-1}s^{-1}$ at 245K. The value increases gradually to 7.6×10^{-4} $cm^2V^{-1}s^{-1}$ at 373K. However, for the control device, the hole mobilities are about a half order less from 3.3×10^{-5} to 2.2×10^{-4} $cm^2V^{-1}s^{-1}$ in the same temperature range.

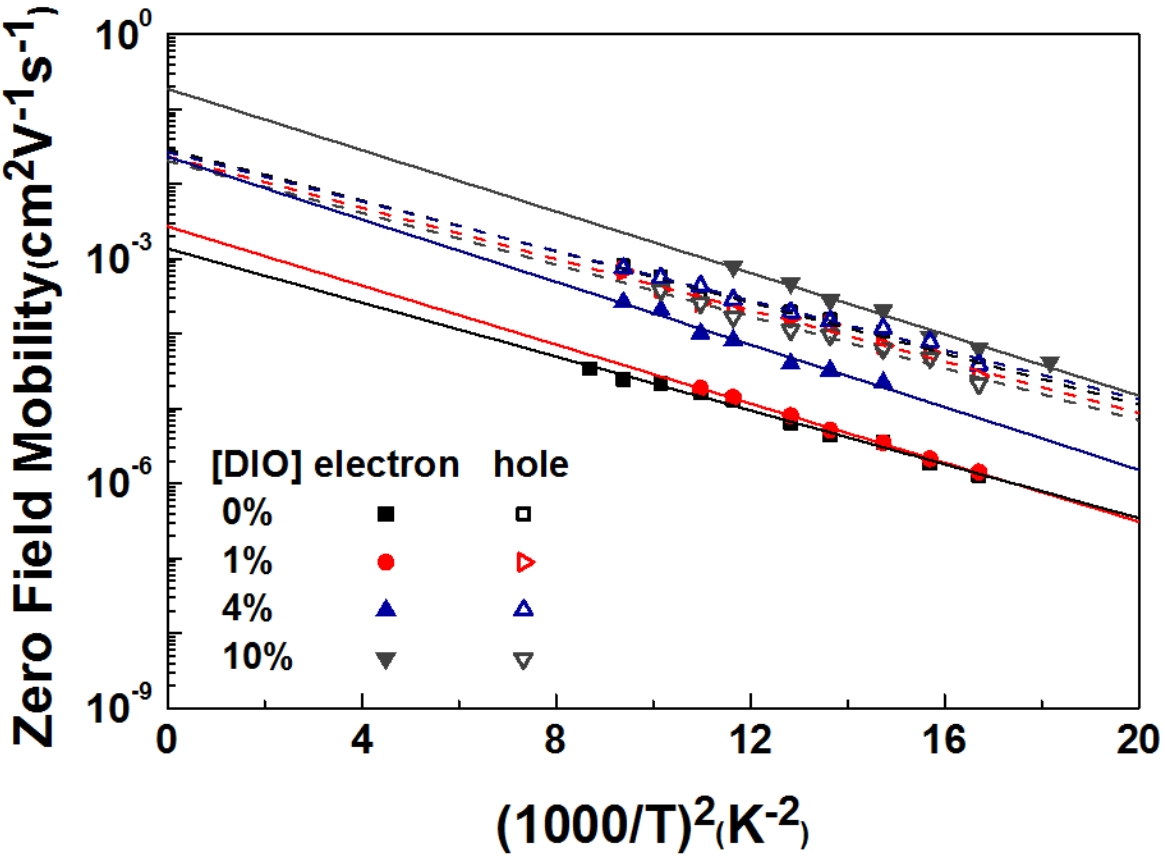

Figure 4. Zero-field carrier mobilities of PTB7:$PC_{71}BM$ polymer-rich BHJ devices vs $1/T^2$ of PTB7:$PC_{71}BM$ OPV devices using AS derived data. Dashed and solid lines are the best linear fits to the experimental data using Equation 3. The slopes of the plots yield the energetic disorders and the y-intercepts yield the high temperature limits of the carrier mobilities. Note the hole data almost overlap with each other; the electron mobilities increase by about 2 orders of magnitude from 0 to 10% DIO in the casting solutions.

Figure 5 can be used to describe and analyze the balance of electron and hole mobilities in the PTB7:$PC_{71}BM$ BHJs. When DIO is not sufficient in casting solution, the fullerene in the active layer cannot be dispersed adequately after spin coating, resulting in the lower electron mobility than hole. So, the DIO concentration can be employed as a means to tune the electron mobility in the DIO. Increasing DIO concentration leads to a substantial increase in

μ_e However, there is little impact on μ_h. Thus, the hole mobility would be much lower than electron mobility if we add excessive DIO. When we added 4 vol% DIO into the casting solution, electron mobility can be on par with hole mobility μ_h with the value of about 3×10^{-4} $cm^2V^{-1}s^{-1}$, under which the PCE of device can reach a peak value of 7.7% as indicated in Figure 1.

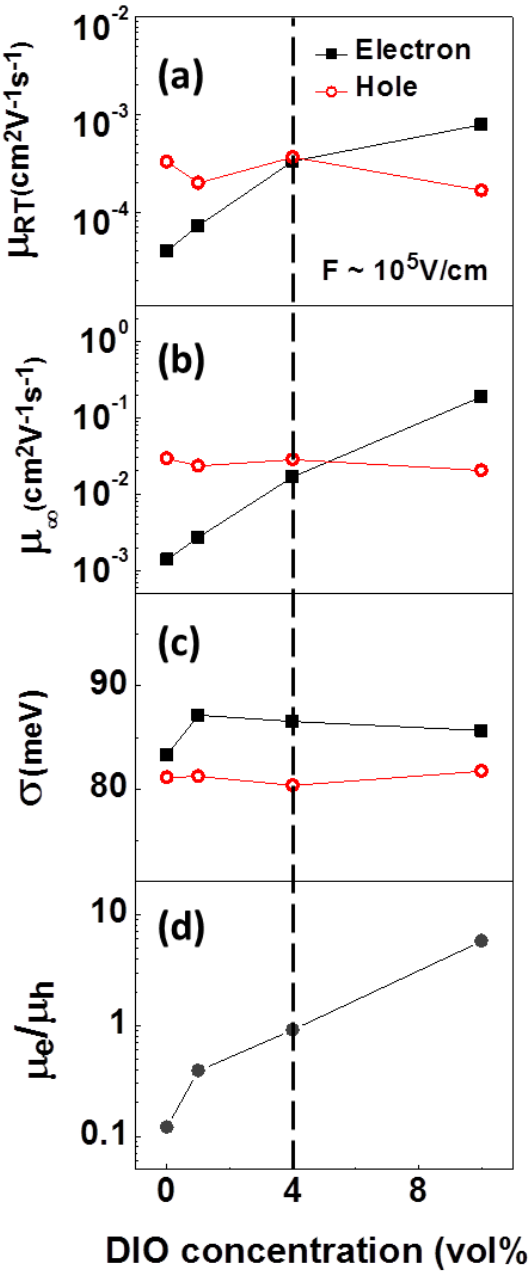

Figure 5. Summary plots for transport parameters for the PTB7:$PC_{71}BM$ polymer-rich BHJ

films for different DIO concentrations: (a) Room temperature mobilities, (b) High temperature limits of the mobilities, (c) Energetic disorders, (d) Ratio of electron-to-hole mobilities at F≈10^5 V/cm conditions at room temperature. The vertical dashed line indicates the DIO concentration (4%) chosen for the optimized PTB7:$PC_{71}BM$ polymer-rich BHJ.

2.3. Polymer-rich Strategy for PCDTBT:$PC_{71}BM$ and PDTSTPD:$PC_{71}BM$ BHJ Systems

To further investigate the universality of the polymer-rich strategy, we chose other two polymer:$PC_{71}BM$ systems including PCDTBT and PDTSTPD. The J-V curves of optimal PCDTBT:$PC_{71}BM$ and PDTSTPD:$PC_{71}BM$ BHJ OPV devices with different D:A weight ratios are shown in **Figure 6(a)**. Likewise the PTB7:$PC_{71}BM$ system in Section 2.1, the polymer-rich PCDTBT:$PC_{71}BM$ and PDTSTPD:$PC_{71}BM$ solar cells have larger J_{sc}s, with roughly equal levels of V_{oc}s and FFs, resulting in better OPV performances. The OPV parameters are shown in **Table 2**. It is worth noting that the polymer-rich strategy also works for the PCDTBT:$PC_{71}BM$ system, where the DIO does not exist in the control BHJ film. When the D:A weight ratio changes from 1:4 to 1:1.25, the Jsc increases from 10.5 mA/cm^2 to 11.3 mA/cm^2, with a higher PCE of 6.3% (control of 5.9%). The corresponding EQE spectra [**Figure 6(b)**] of two polymer:$PC_{71}BM$ devices indicate that the EQE enhancements are mainly in the wavelength regions where the polymers can absorb more incident light.

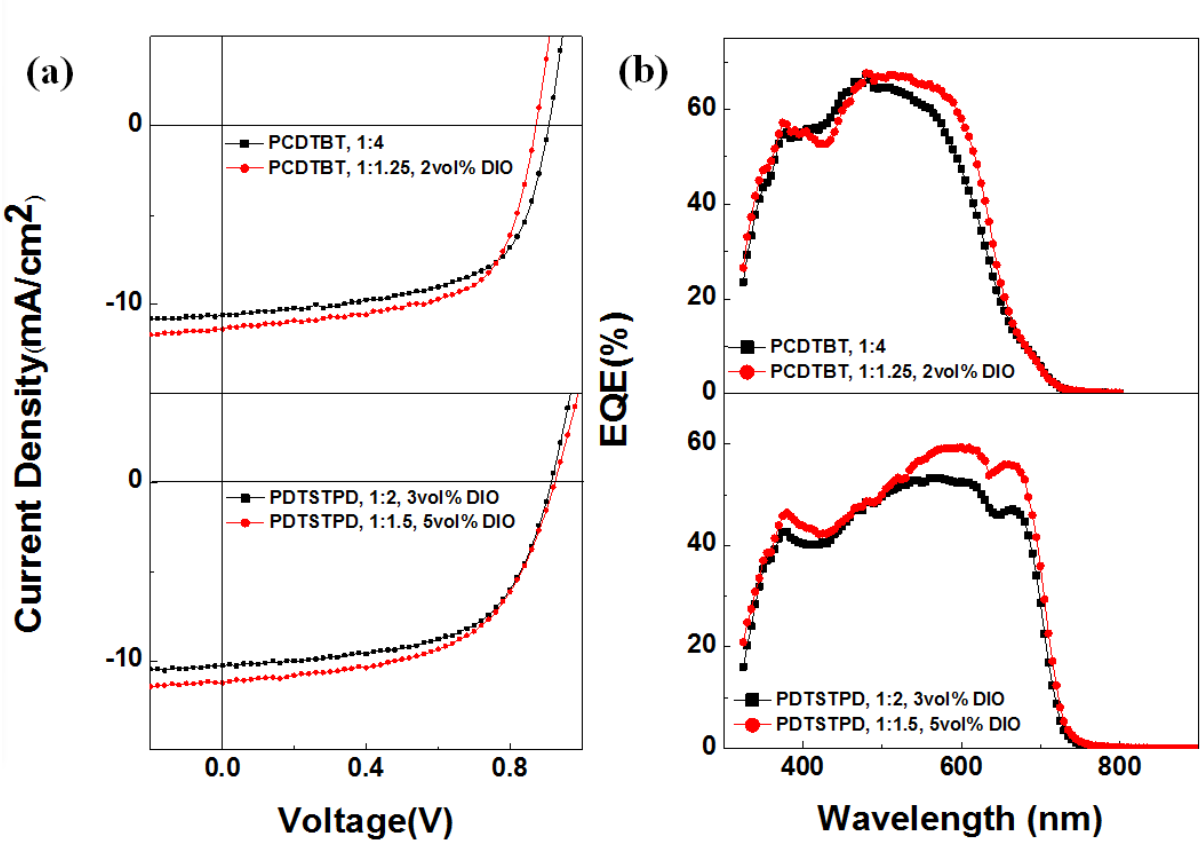

Figure 6. (a) JV data of typical PCDTBT:$PC_{71}BM$ and PDTSTPD:$PC_{71}BM$ BHJ OPV devices under 100 mW/cm^2 of AM1.5G solar illumination. The data points in circles indicate BHJ cells with enhanced polymer contents; the data points in squares are the control devices. The D:A ratios are indicated in each plot; (b) EQE spectra for PCDTBT:$PC_{71}BM$ and PDTSTPD:$PC_{71}BM$ BHJ OPV devices;

Figure 7(a) and **Fig 7(b)** are the UV-visible absorption spectra and the JV data of hole-only devices of the PCDTBT:$PC_{71}BM$ and PDTSTPD:$PC_{71}BM$ BHJ films. Both the PCDTBT:$PC_{71}BM$ and PDTSTPD:$PC_{71}BM$ BHJ films exhibit enhanced hole mobilities. For example, the hole mobility of PCDTBT:$PC_{71}BM$ increases gradually from around 3.2×10^{-6} $cm^2V^{-1}s^{-1}$ to around 2.3×10^{-5} $cm^2V^{-1}s^{-1}$, about one order larger when the D:A ratio increases from 1:4 to 1:1.25. Table 1, last column, is a summary of the SCLC fittings.

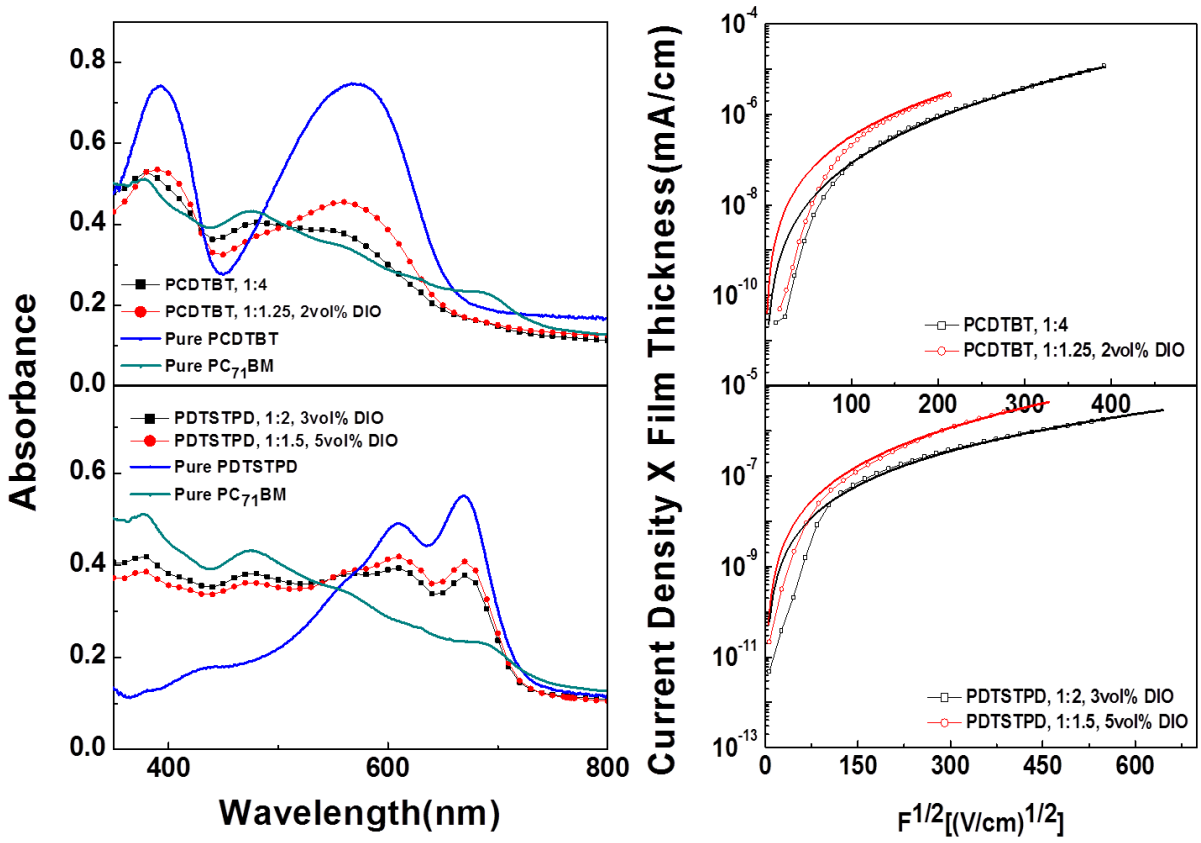

Figure 7. (a) UV-visible absorption spectra for PCDTBT:$PC_{71}BM$ and PDTSTPD:$PC_{71}BM$ BHJ films and materials absorption spectra with thicknesses similar to their BHJ cells; (d) Current vs applied field data for PCDTBT:$PC_{71}BM$ and PDTSTPD:$PC_{71}BM$ BHJ hole-only devices at room temperature. Circles are data for the polymer-rich samples while squares are data for the control devices. Solid lines are SCLC fittings using Equation 1.

BHJ	D:A weight ratio	DIO concentration (in vol%)	J_{sc} (mA/cm^2)	V_{oc} (V)	FF (%)	PCE (%)	μ_0(cm^{2}V^{-1}s^{-1})
PCDTBT:	1:1.25	2	11.3	0.88	63	6.3	2.4×10^{-5}
$PC_{71}BM$	1:4	0	10.5	0.90	61	5.9	3.2×10^{-6}
PDTSTPD:	1:1.5	5	11.6	0.92	59	6.3	6.4×10^{-6}
$PC_{71}BM$	1:2	3	10.3	0.91	60	5.6	3.9×10^{-6}

Table 2. Summary of performances of bulk-heterojunction OPV devices for different D:A ratios using PCDTBT and PDTSTPD as the donor polymers. The last column indicates the hole mobilities obtained from SCLC fittings (Equation 1) to the JV data.

3. Conclusion

In this report, we have enriched the polymer contents of the BHJs of PTB7:$PC_{71}BM$, PCDTBT:$PC_{71}BM$ and PDTSTPD:$PC_{71}BM$ with various DIO concentrations. (**Figure. 8**) For the three BHJs with hole mobilities ~ 10^{-6} to 10^{-4} cm^{2}V^{-1}s^{-1}, polymer-rich devices can be fabricated with better PCEs and short circuit currents, comparing with control cells. To further explain the performance enhancement of OPV devices, the transport properties and optical absorptions of BHJs were investigated. Hole mobilities can be improved when we modified the D:A ratios. At the same time, the electron mobilities can be still on par with the hole mobility by tuning the DIO concentrations in the processing solution. We also observe that there are also improvements for the optical absorptions of BHJ layers due to the increase of polymer contents. This work demonstrates that the acceptor concentrations in commonly

used BHJs can be reduced with better performance due to better balanced carrier mobilities and improvement of optical absorptions**.**

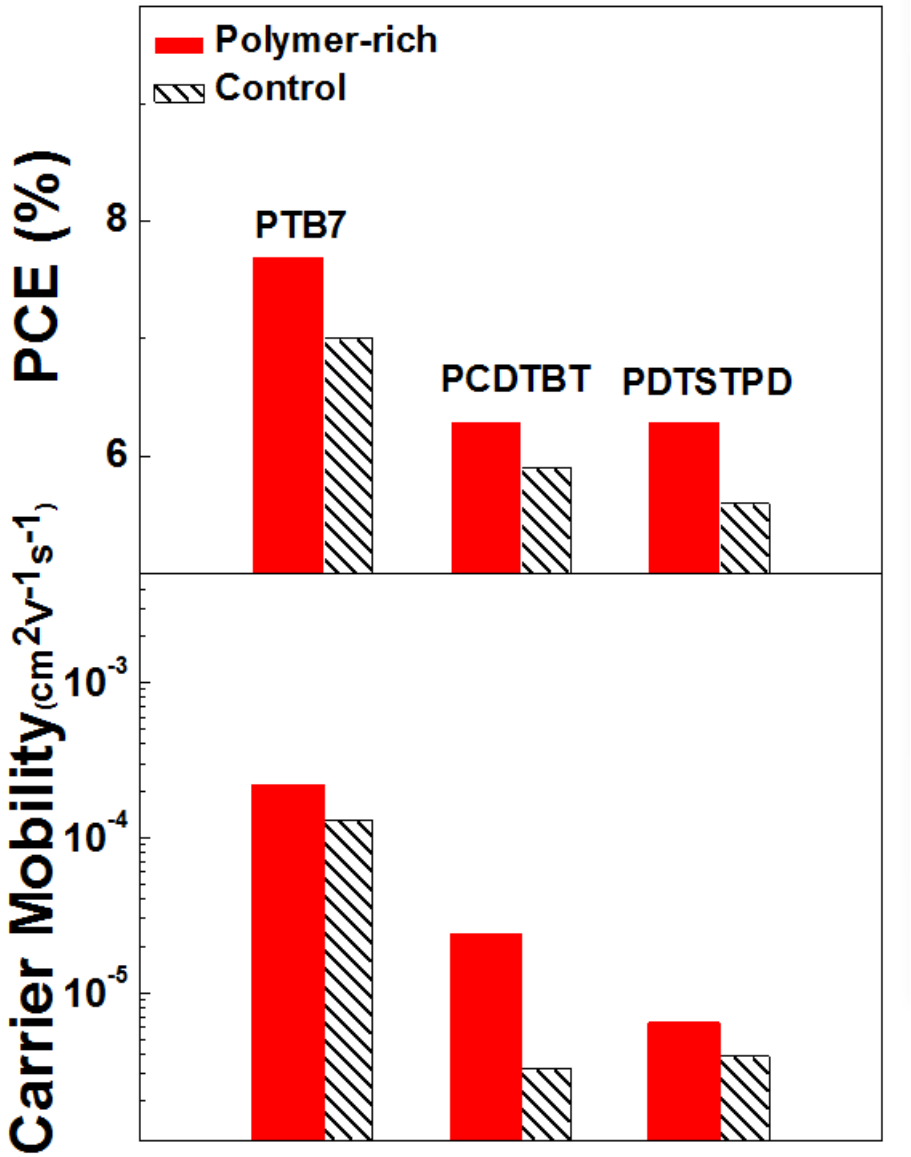

Figure 8. (a) PCEs of BHJs with enriched polymer contents with increased DIO concentrations (filled bars). These devices were made using higher DIO concentrations in their casting solutions. (b) The hole mobilities of their BHJ films. Control devices of BHJ films are shown as shaded bars.

4. Experimental Section

Materials: PTB7, PCDTBT and PDTSTPD were purchased from 1-Material. $PC_{71}BM$, and PEDOT:PSS were obtained from Chemical Industry Co., Sigma-Aldrich, Luminescene Technology, respectively. These materials were used as received. CuPc was purchased from Sigma-Aldrich and was further purified by vacuum sublimation.

PTB7 and PDTSTPD OPV Cell Fabrication and Characterization: The ITO patterned glass substrate was sequentially cleaned by deionized water, acetone, and 2-propanol in ultrasonic bath for 40 min respectively. After a UV ozone cleaning treatment, a 30nm PEDOT:PSS buffer layer was spin coated on the substrate, followed by annealing for 10 min at 140°C. The sample was then transferred into the nitrogen glovebox. Polymers and $PC_{71}BM$ were dissolved in chlorobenzene (CB) with different mass ratios and spin coated to form different thicknesses of BHJ films. The sample was dried at room temperature overnight and then transferred into the high vacuum chamber to evaporate the LiF and aluminium layers. The final structure of the organic solar cell was ITO/PEDOT:PSS/BHJ/LiF/Al. An AM 1.5G simulator with the light intensity of $100mW/cm^2$ was used to measure the characteristic of the OPV sample.

PCDTBT OPV Cell Fabrication: The substrate was transferred into the high vacuum chamber to evaporate a 10nm MoO_3 layer directly, to alternate the layer of PEDOT:PSS. Then the preparation process was similar with the PTB7, PTB7-Th and PDTSTPD device fabrication. The structure of the PCDTBT OPV device was ITO/ MoO_3/BHJ/LiF/Al.

Hole and Electron Transport Measurements: The preparation method of the single-carrier-only device was similar to that of the OPV cell. The structure of the hole-only

device was ITO/Buffer Layer/BHJ/CuPc:Spiro-TPD/Au, and the structure of the electron-only device was ITO/Al/BHJ/LiF/Al.

Supporting Information

- AFM morphology images;

-Admittance spectroscopy curves;

(a)

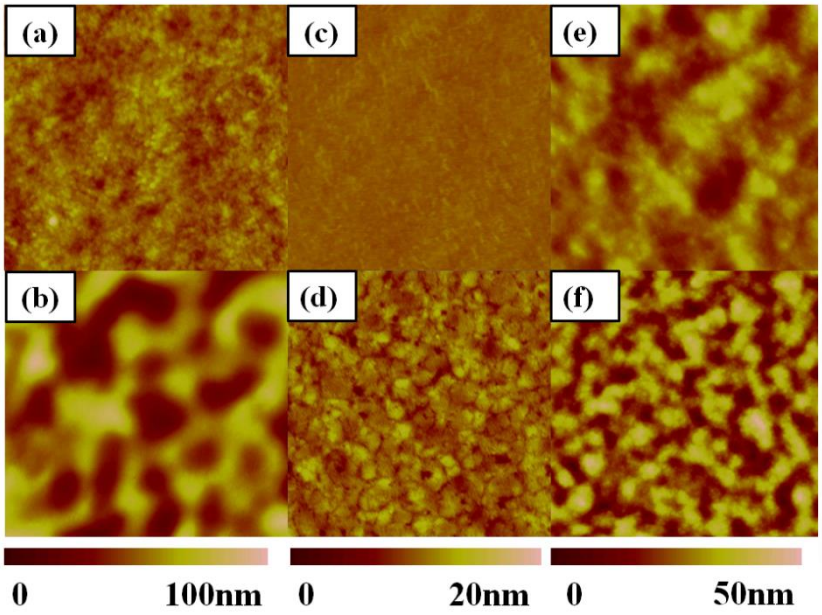

Figure S1. AFM morphology images (2μm ×2μm) height for (a)(b)PTB7:$PC_{71}BM$, (c)(d)PCDTBT:$PC_{71}BM$ and (e)(f)PDTSTPD:$PC_{71}BM$ BHJ polymer-rich and control BHJ films. (a)(c)(d) are the polymer-rich BHJ films, while (b)(d)(f) are the control BHJ films.

(a)

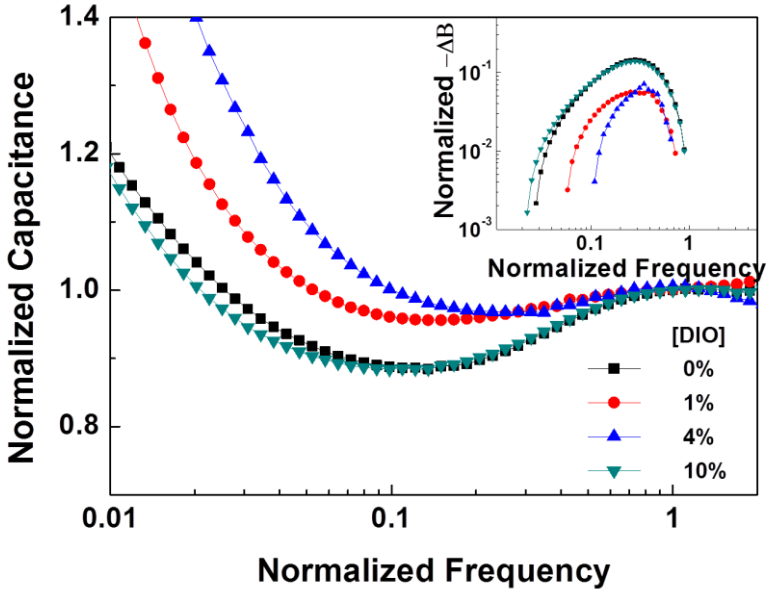

(b)

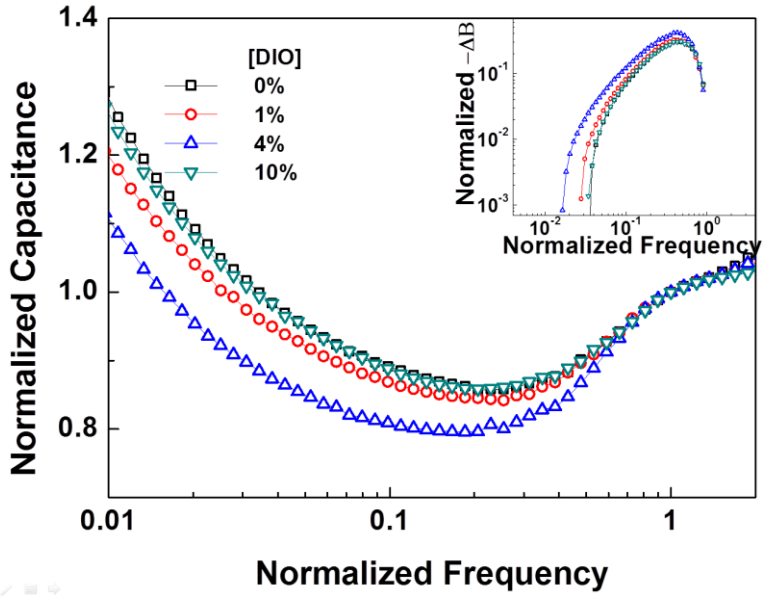

Figure S2. Capacitance versus frequency plots for (a) electron and (b) hole-only devices with 0, 1, 4 and 10 vol% DIO at room temperature. The insets shows the negative susceptance versus frequency plots of corresponding mobilities.

BHJ	D:A weight ratio	DIO concentration (in vol%)	J_{sc} (mA/cm^2)	V_{oc} (V)	FF (%)	PCE (%)
PTB7: $PC_{71}BM$	1:1.5	3	15.1	0.77	60	7.0
	1:1	4	16.8	0.78	59	7.7
	1:1	6	16.5	0.77	56	7.1
	1:1	8	16.0	0.78	59	7.3
	1:0.8	4.5	15.7	0.78	56	6.9
	1:0.8	8	15.3	0.77	56	6.6
	1:0.6	8	12.6	0.77	52	5.0

BHJ	D:A weight ratio	DIO concentration (in vol%)	J_{sc} (mA/cm^2)	V_{oc} (V)	FF (%)	PCE (%)
PCDTBT: $PC_{71}BM$	1:4	0	10.6	0.90	61	5.9
	1:3	0	10.9	0.88	61	5.9
	1:2	0	10.8	0.88	60	5.7
	1:.25	0	11.5	0.92	52	5.5
	1:1.25	2	11.4	0.88	63	6.3
	1:1.25	4	10.9	0.88	62	5.9
	1:1	5	10.0	0.88	51	4.4

BHJ	D:A weight ratio	DIO concentration (in vol%)	J_{sc} (mA/cm^2)	V_{oc} (V)	FF (%)	PCE (%)
PDTSTPD: $PC_{71}BM$	1:2	3	10.3	0.91	60	5.6
	1:1.5	5	11.6	0.92	59	6.3
	1:1	5	11.1	0.93	51	5.3

Table S1. Optimization procedures of PTB7:$PC_{71}BM$, PCDTBT:$PC_{71}BM$ and PDTSTPD:$PC_{71}BM$ OPV devices with different D:A ratios and DIO concentrations.

Appendix 1. Admittance Spectroscopy Analysis of Charge Carrier Transport[27,28]

Admittance spectroscopy (AS) is a technique for the measurement of carrier mobility in organic materials. For a given organic BHJ layer which is located between two electrodes with a thickness *d* and a permittivity ε, carriers can transport through the BHJ film and then be injected to corresponding electrode (an Ohmic contact is formed), whereas the undesirable carriers can be blocked by the blocking layer of the other electrode. Based on the DC voltage, if another small AC perturbation is added to the sample, the frequency dependent admittance $Y(\omega)$ can be expressed as,

$$Y(\omega) = G + jS = j\omega C$$

where G is the conductance, S is the susceptance, C is the capacitance, j is the imaginary number, and ω is the angular frequency.

The carrier mobility then can be analyzed by the capacitance as a function of frequency. The average carrier mobility μ_{dc} can be extracted as,

$$\mu_{dc} = \frac{d^2}{0.56\tau_r(V - V_{bi})}$$

where *d* is the thickness of the BHJ layer, V_{bi} is the built-in voltage, *V* is the applied voltage and τ_r is the average carrier flight-time.

Figure S1 shows the frequency-dependent capacitances. From the data, the negative differential susceptance $-\Delta B$ vs frequency plot can be deduced. The maximum value of $-\Delta B$ can be used to extract the carrier transit times. The carrier transit time τ_r can be computed by the equation $\tau_r = 0.56 f_r^{-1}$. Finally, the carrier mobilities can be calculated by the relationship of $u_{dc} = d^2/\tau_r V_{dc}$, where the V_{dc} is the direct current biased voltage and d is the thickness of BHJ layer.

AUTHOR INFORMATION

Corresponding Author

Shu Kong So*

Email: skso@hkbu.edu.hk

Contact Number: (+852) 3411-7038

Address: Department of Physics and Institute of Advanced Materials

Hong Kong Baptist University

Kowloon Tong, Hong Kong SAR, P.R. China

Funding Sources

The Research Committee of HKBU under RC-ICRS/15-16/4A and the Theme-based Research Scheme (TBRS) Grant #T23-713/11.

ACKNOWLEDGMENT

Support of this work by the Research Committee of HKBU under RC-ICRS/15-16/4A and the Theme-based Research Scheme (TBRS) Grant # T23-713/11 are gratefully acknowledged.

REFERENCES

(1) M. C. Scharber; N. S. Sariciftci. Efficiency of Bulk-heterojunction Organic Solar Cells. *Prog. Polym. Sci.* **2013**, *38*, 1929-1940.

(2) Q. An, F. Zhang, J. Zhang, W. Tang, Z. Deng, B. Hu. Versatile Ternary Organic Solar Cells: a Critical Review. *Energy Environ. Sci.* **2016**, *9*, 281-322.

(3) I. Etxebarria, J. Ajuria, R. Pacios. Solution-processable Polymeric Solar Cells: a Review on Materials, Strategies and Cell Architectures to Overcome 10%. *Org. Electron*. **2015**, *19*, 34-60.

(4) T. Kirchartz, K. Taretto, U. Rau. Efficiency Limits of Organic Bulk Heterojunction Solar Cells. *J. Phys. Chem*. **2009**, *113*, 17958-17966.

(5) Y. W. Su, S. C. Lan, K. H. Wei. Organic Photovoltaic. *Mater. Today*. **2012**, *15*, 554-562.

(6) H. C. Weerasinghe, N. Rolston, D. Vak, A. D. Scully; R.H. Dauskardt. A stability study of roll-to-roll processed organic photovoltaic modules containing a polymeric electron-selective layer *Sol. Energ. Mat. Sol. C.* **2016**, *152*, 133-140.

(7) K. Hwang, Y. Jung, Y. Heo, F. H. Scholes, S. E. Watkins, J. Subbiah, D. J. Jones, D. Kim, D. Vak. Toward Large Scale Roll-to-Roll Production of Fully Printed Perovskite Solar Cells. *Adv. Mater*. **2015**, *27*, 1241-1247.

(8) H. Zhang, W. Tan, S. Fladischer, L. Ke, T. Ameri, N. Li, M. Turbiez, E. Spiecker, X. Zhu, Y. Cao, C. J. Brabec. Roll to Roll Compatible Fabrication of Inverted Organic Solar Cells with a Self-organized Charge Selective Cathode Interfacial Layer. *J. Mater. Chem. A.* **2016**, *4*, 5032-5038.

(9) G. Li, R, Zhu, Y. Yang Polymer Solar Cells. *Nat. Photonics*. **2012**, *6*, 153-161.

(10) G. Namkoong, J. Kong, M. Samson, I. Hwang, K. Lee. Active Layer Thickness Effect on the Recombination Process of PCDTBT:$PC_{71}BM$ Organic Solar Cells. *Org. Electron*. **2013**, *14*, 74-79.

(11) C. J. Brabec, S. Gowrisanker , J. J. M. Halls, D. Laird, S. Jia, S. P. Williams. Polymer-Fullerene Bulk-Heterojunction Solar Cells. *Adv. Mater*. **2010**, *22*, 3839-3856.

(12) P. W. M. Blom, V. D. Mihailetchi, L. J. A. Koster, D. E. Markov. Device Physics of Polymer:Fullerene Bulk Heterojunction Solar Cells. *Adv. Mater*. **2007**, *19*, 1551-1566.

(13) Y. Y. Liang, Z. Xu, J. B. Xia, S. T. Tsai, Y. Wu, G. Li, C. Ray, L. P. Yu. For the Bright Future – Bulk Heterojunction Polymer Solar Cells with Power Conversion Efficiency of 7.4%. *Adv. Mater*. **2010**, *22*, E135-E138.

(14) S. Ochiai, S. Imamura, S. Kannappan, K. Palanisamy, P. Shin. Characteristics and the Effect of Additives on the Nanomorphology of PTB7/$PC_{71}BM$ Composite Films. *Curr. Appl. Phys*. **2013**, *13*, S58-S63.

(15) X. Zhao, J. Xiang, D. Liu, D. Zhou, G. Wang, G. Zhou, K. Alameh, B. Ding, Q. Song. Impact of alkyl chain length of 1,*n*-diiodoalkanes on PC71BM distribution in both bulk and air surface of PTB7:PC71BM film. *Org. Electron*. **2016**, *37*, 358-365.

(16) Z. C. He, C. M. Zhong, S. J. Su, M. Xu, H. B. Wu, Y. Cao. Enhanced Power-conversion Efficiency in Polymer Solar Cells Using an Inverted Device Structure. *Nat. Photon.* **2012**, *6*, 591-595.

(17) S. H. Park, A. Roy, S. Beaupre, S. Cho, N. Coates, J. S. Moon, D. Moses, M. Leclerc, K. Lee, A. J. Heeger. Bulk Heterojunction Solar Cells with Internal Quantum Efficiency Approaching 100%. *Nat. Photonics.* **2009**, *3*, 297-302.

(18) D. Qian, W. Ma, Z. Li, X. Guo, S. Zhang, L. Ye, H. Ade, Z. Tan, J. Hou. Molecular Design toward Efficient Polymer Solar Cells with High Polymer Content. *J. Am. Chem. Soc*. **2013**, *135*, 8464-8467.

(19) J. Yuan, H. Dong, M. Li, X. Huang, J. Zhong, Y. Li, W. Ma. High Polymer/Fullerene Ratio Realized in Efficient Polymer Solar Cells by Tailoring of the Polymer Side-Chains. *Adv. Mater*. **2014**, *26*, 3624-3630.

(20) A. C. Mayer, M. F. Toney, S. R. Scully, J. Rivnay, C. J. Brabec, M. Scharber, M. Koppe, M. Heeney, I. McCulloch, M. D. McGehee. Bimolecular Crystals of Fullerenes in Conjugated Polymers and the Implications of Molecular Mixing for Solar Cells. *Adv. Funct. Mater*. **2009**, *19*, 1173-1179.

(21) H. K. H. Lee, K. K. H. Chan, S. K. So. Role of Electron Blocking and Trapping Layers in Transport Characterization of a Photovoltaic Polymer Poly(3-hexylthiophene). *Org. Electron*. **2012**, *13*, 541-544.

(22) C. H. Y. Ho, Q. Dong, H. Yin, W. W. K. Leung, Q. Yang, H. K. H. Lee, S. W. Tsang, S. K. So. Impact of Solvent Additive on Carrier Transport in Polymer:Fullerene Bulk Heterojunction Photovoltaic Cells. *Adv. Mater. Interfaces*. **2015**, *2*, 1500166.

(23) H. K. H. Lee, Z. Li, I. Constantinou, F. So, S. W. Tsang, S. K. So. Batch-to-Batch Variation of Polymeric Photovoltaic Materials: its Origin and Impacts on Charge Carrier Transport and Device Performances. *Adv. Energy Mater*. **2014**, *4*, 1400768.

(24) M. Lampert, P. Mark. *Current Injection in Solids*, Academic Press, New York, USA **1970**.

(25) P. N. Murgatroyd. *J. Phys. D: Appl. Phys.* **1970**, *3*, 151.

(26) K. K. H. Chan, S. W. Tsang, H. K. H. Lee, F. So, S. K. So. Charge Transport Study of Semiconducting Polymers and Their Bulk Heterojunction Blends by Capacitance Measurements. *J. Polym. Sci., Part B: Polym. Phys.* **2013**, *51*, 649-658.

(27) S. W. Tsang, S. K. So, J. B. Xu. Application of Admittance Spectroscopy to Evaluate Carrier Mobility in Organic Charge Transport Materials. *J. Appl. Phys*. **2006**, *99*, 013706.

(28) K. K. Tsung, S. K. So. Advantages of Admittance Spectroscopy over Time-of-flight Technique for Studying Dispersive Charge Transport in an Organic Semiconductor. *J. Appl. Phys*. **2009**, *106*, 083710.

(29) H. C. F. Marten, H. B. Brom, P. W. M. Blom. Simultaneous Measurement of Electron and Hole Mobilities in Polymer Light-emitting Diodes. *Appl. Phys. Lett*. **2000**, *77*, 1852.

(30) H. Gommans, M. Kemerink, G. G. Andersson, R. M. T. Pijper. Charge Transport and Trapping in Cs-doped Poly(dialkoxy-*p*-phenylene vinylene) Light-emitting Diodes. *Phys. Rev. B*. **2004**, *69*, 155216.

(31) S. Foster, F. Deledalle, A. Mitani, T. Kimura, K. Kim, T. Okachi, T. Kirchartz, J. Oguma, K. Miyake, J.R. Durrant, S. Doi, J. Nelson. Electron Collection as a Limit to Polymer:PCBM Solar Cell Efficiency: Effect of Blend Microstructure on Carrier Mobility and Device Performance in PTB7:PCBM. *Adv. Energy Mater*. **2014**, *4*, 1400311.

(32) H. Bassler. Charge Transport in Disordered Organic Photoconductors a Monte Carlo Simulation Study. *Phys. Status Solidi B*. **1993**, *175*, 15-56.